Available online at www.sciencedirect.com
ScienceDirect
Advances in Space Research 48 (2011) 1551–1564
ADVANCES IN SPACE RESEARCH (a COSPAR publication)
www.elsevier.com/locate/asr

A feasibility study for the detection of the diurnal variation of tropospheric NO_2 over Tokyo from a geostationary orbit

Katsuyuki Noguchi [a,*,1], Andreas Richter [a], Heinrich Bovensmann [a], Andreas Hilboll [a], John P. Burrows [a], Hitoshi Irie [b], Sachiko Hayashida [c], Yu Morino [d]

[a] Institute of Environmental Physics, University of Bremen, P.O. Box 33 04 40, 28334 Bremen, Germany
[b] Japan Agency for Marine-Earth Science and Technology, 3173-25 Showamachi, Kanazawa-ku, Yokohama, Kanagawa 236-0001, Japan
[c] Nara Women's University, Kita-uoya Nishi-machi, Nara 630-8506, Japan
[d] National Institute for Environmental Studies, 16-2 Onogawa, Tsukuba, Ibaraki 305-8506, Japan

Received 28 December 2010; received in revised form 27 June 2011; accepted 28 June 2011
Available online 5 July 2011

Abstract

We have conducted a feasibility study for the geostationary monitoring of the diurnal variation of tropospheric NO_2 over Tokyo. Using NO_2 fields from a chemical transport model, synthetic spectra were created by a radiative transfer model, SCIATRAN, for summer and winter cases. We then performed a Differential Optical Absorption Spectroscopy (DOAS) analysis to retrieve NO_2 slant column densities (SCDs), and after converting SCDs into vertical column densities (VCDs), we estimated the precision of the retrieved VCDs. The simulation showed that signal-to-noise ratio (SNR) $\geqslant$ 500 is needed to detect the diurnal variation and that SNR $\geqslant$ 1000 is needed to observe the local minimum occurring in the early afternoon (LT13–14) in summer. In winter, the detection of the diurnal variation during LT08–15 needs SNR $\geqslant$ 500, and SNR $\geqslant$ 1000 is needed if early morning (LT07) and early evening (LT16) are included. The currently discussed sensor specification for the Japanese geostationary satellite project, GMAP-Asia, which has a horizontal resolution of 10 km and a temporal resolution of 1hr, has demonstrated the performance of a precision of several percent, which is approximately corresponding to SNR = 1000–2000 during daytime and SNR $\geqslant$ 500 in the morning and evening. We also discuss possible biases caused by the temperature dependence of the absorption cross section utilized in the DOAS retrieval, and the effect of uncertainties of surface albedo and clouds on the estimation of precisions.

Keywords: Geostationary satellite; Nitrogen dioxide; Feasibility study

1. Introduction

Nitrogen oxides ($NO_x = NO + NO_2$) are well-known anthropogenic air pollutants emitted in the process of fossil fuel combustion from power plants and vehicles mainly in the form of NO. NO_x itself is harmful to human health and has a key role in the formation of tropospheric ozone, which is also toxic to the human body and the dominant component of photochemical smog; the photolysis of NO_2 first produces $O(^3P)$ and NO, and a three-body reaction including $O(^3P)$ quickly forms ozone. The NO formed in the photolysis of NO_2 would oxidize ozone again without other reactions. In polluted air, however, NO is successively oxidized by radical compounds such as organic peroxy radical (RO_2) and the hydroperoxyl radical (HO_2) before consuming ozone, and ozone formation can proceed without consuming ozone (Hobbs, 2000).

* Corresponding author.
E-mail addresses: nogu@ics.nara-wu.ac.jp (K. Noguchi), Andreas.Richter@iup.physik.uni-bremen.de (A. Richter), Heinrich.Bovensmann@iup.physik.uni-bremen.de (H. Bovensmann), hilboll@iup.physik.uni-bremen.de (A. Hilboll), burrows@iup.physik.uni-bremen.de (J.P. Burrows), irie@jamstec.go.jp (H. Irie), sachiko@ics.nara-wu.ac.jp (S. Hayashida), morino.yu@nies.go.jp (Y. Morino).
[1] On leave from Nara Women's University (Kita-uoya Nishi-machi, Nara 630-8506, Japan) during 2008–2010.

0273-1177/$36.00 © 2011 COSPAR. Published by Elsevier Ltd. All rights reserved.
doi:10.1016/j.asr.2011.06.029

Since the mid 1990s, space-borne measurements based on spectroscopic techniques have been developed to complement the ground-based monitoring network. The Global Ozone Monitoring Experiment (GOME) (Burrows et al., 1999) and its successor Scanning Imaging Absorption Spectrometer for Atmospheric Cartography (SCIAMACHY) (Bovensmann et al., 1999) are the pioneers for the global tropospheric trace gas measurements from space using backscattered solar radiation. The measurements of GOME and SCIAMACHY revealed global long-term trends in the tropospheric NO_2 including China, where a large increase rate of the tropospheric NO_2 was found (Richter et al., 2005), constraints for the global inventories of NO_x emissions (Leue et al., 2001; Martin et al., 2003), and global distributions of NO_x sources by the identification of the seasonal cycles of the sources (van der et al., 2008). Following GOME and SCIAMACHY, measurements with improved spatial resolutions and more frequent global surface coverage are performed by the Ozone Monitoring Instrument (OMI) (Levelt et al., 2006) and GOME-2 (Callies et al., 2000). The observations from OMI and GOME-2 facilitate studying the spatiotemporal distribution of the tropospheric NO_2 over urban and industrialized regions (Wang et al., 2007; Kim et al., 2009; Mijling et al., 2009; Sitnov, 2009; Witte et al., 2009; Zhang et al., 2009).

The satellites carrying those sensors have sun-synchronous low earth orbits (LEO), and the observations of a given location would be conducted at a fixed local time (except at high latitudes where several orbits from the same day overlap) when only one sensor was utilized. Therefore, the measurements based on only one sensor cannot obtain the information on the diurnal variation of a species. To overcome this limitation of the observation with one sensor, a satellite constellation with several instruments was utilized. Boersma et al. (2008) showed that the difference of NO_2 observed by SCIAMACHY (observing at LT10–11) and OMI (at LT13–14) is up to 40% in summer, depending on the sources of NO_2. The authors attributed the difference between SCIAMACHY and OMI's results primarily to daytime photochemical loss of NO_2, weakened by a broad daytime maximum of anthropogenic NO_x emissions. Boersma et al. (2009) showed further detailed results on the seasonal difference of the diurnal variations of the tropospheric NO_2 over urban areas; SCIAMACHY (observing at LT10–11) > OMI (at LT13–14) in summer but vice versa in winter. The authors discussed the reason of the seasonal difference using a chemical transport model (CTM) and concluded that the seasonally varying photochemistry mainly causes the difference. Such a satellite constellation with instruments in morning and noon orbits has contributed to the understanding on the most important diurnal trends in chemistry and emissions. It could further be complemented if measurements from additional instruments in the afternoon were available.

In contrast to LEO, a geostationary earth orbit (GEO) enables hourly measurements throughout the day. Hourly observations with GEO are particularly useful for the study of the diurnal variation of tropospheric species such as NO_2 because;

- data from one instrument are more consistent than data from a constellation,
- hourly data can track emissions e.g. during rush hours which is not possible with a constellation, and
- hourly data at high spatial resolution allow tracking of transport.

Hourly NO_2 data from a geostationary sensor ingested into data assimilation systems could also provide the necessary input to take air quality forecasts further and improve them up to the point that they can reliably forecast violations of air quality standard hours in advance. A GEO measurement has another advantage against the existing satellite constellation; GEO can solve a temporal sampling problem of the existing LEO measurements. We define the temporal sampling problem of LEO as the shortage of the temporal frequency in observations. The LEO observations of a given location are conducted once per day at most. As clouds often prevent measurements down to the surface, the real sampling frequency at a given location tends to be reduced to less than once per day. The introduction of GEO can create a much larger number of cloud free observations, solving the temporal sampling problem of the existing LEO measurements. Note that the introduction of GEO would result in another problem: a spatial sampling problem. Since GEO instruments can only cover part of the Earth, they introduce a spatial sampling problem in that the rest of the Earth is not covered at all. Therefore, while solving the temporal sampling problem, the use of a GEO-instrument generates a spatial sampling problem. Indeed, the existing LEO measurements had a priority on solving the spatial sampling problem and obtained a global coverage of the tropospheric NO_2. To solve the spatial sampling problem in a GEO-based measurement system, several simultaneous measurements, e.g., in Asia, Europe and America will be needed. As an alternative, GEO and LEO observations can be combined to create a complete global picture.

Since the beginning of the last decade, the possibility of GEO-based measurements of tropospheric tracers has been discussed as a contribution to the local- and regional scale air quality monitoring and forecasts (Kelder et al., 2005; Edwards, 2006). In these discussions, several GEO missions such as GEO TROPSAT (Little et al., 1997) and GeoTROPE (Bovensmann et al., 2002; Burrows et al., 2004) were proposed in the past. Presently, the Geostationary Coastal and Air Pollution Events (GEO-CAPE) mission is being studied in the United States, and the Sentinel-4 mission is proceeding for launch in Europe. In Asia, the Korean Geostationary Environment Monitoring Spectrometer (GEMS) is planned to be operating onboard of a GEO satellite. In Japan, the Geostationary Mission for Meteorology and Air Pollution (GMAP-Asia) was proposed by the Japan Society of Atmospheric Chemistry

(Akimoto et al., 2008; Akimoto et al., 2009). In those missions, the development of the sensor is one of the key issues, as the requirements for the sensor specification in GEO (36,000 km altitude) become much more severe than for LEO (<1,000 km) because of the much weaker intensity of light coming from the Earth's atmosphere to GEO.

In the present study, we conducted a feasibility analysis for the detection of diurnal variations of the tropospheric NO_2 from a GEO satellite. As a target region, we focused on Tokyo, which is the largest polluted urban area in Japan. We estimated the precision and its dependence on local time and season by numerical simulations to determine the smallest acceptable signal-to-noise ratio (SNR) for the detector if diurnal variations of NO_2 are to be studied. First, we assume an ideal sensor with constant SNR for the simulations. The results obtained here are general, because no specific sensor specification is assumed in the simulations. Based on these general results, we assume a realistic sensor specification similar to that currently discussed in the GMAP-Asia project and investigate to what extent this hypothetical sensor can detect the diurnal variation of the tropospheric NO_2.

2. Method

In this section, we describe the method used for the simulation conducted in the present study. We refer to the simulation method proposed by Irie et al. (2009). Fig. 1 shows the flow chart of the simulations. First we simulated the Earth's atmospheric radiance spectra as they would be observed in GEO using a radiative transfer model. In the simulation, we implemented the diurnal variations of the vertical profiles of NO_2 for typical summer and winter conditions using numerical simulations. To take into account sensor noise, we added pseudo-noise components to the synthesized spectra. Then, we performed a spectroscopic analysis to retrieve NO_2 slant column densities (SCDs). Finally, we converted the SCDs into vertical column densities (VCDs) by using the stratospheric SCDs and the tropospheric AMF of NO_2, which were derived by SCIATRAN. The tropospheric AMF was calculated by using the exact same atmospheric scenario as used for the calculations of Earth's atmospheric radiance spectra mentioned above. On the other hand, we can immediately calculate the correct VCD by integrating the NO_2 vertical profile for a given atmospheric scenario. We compared the retrieved VCDs with the correct one for error estimation.

2.1. Calculation of the Earth's atmospheric radiance spectra

We calculated the Earth's atmospheric radiance spectra by the radiative transfer model (RTM), SCIATRAN (version 2.2.2), which has been developed to perform radiative transfer modeling for the purpose of measurements of the scattered solar radiation in the Earth's atmosphere (Rozanov et al., 2005). SCIATRAN can perform radiative transfer calculations properly accounting for the spherical shape of the Earth's atmosphere including refraction. In this study, the discrete-ordinates method, which is one of the options provided by SCIATRAN, was selected to solve the integro-differential radiative transfer equation. We calculated the radiance spectra with a wavelength step of 0.1 nm.

As atmospheric scenarios for the input to SCIATRAN, we prepared vertical profiles of the tracers and the

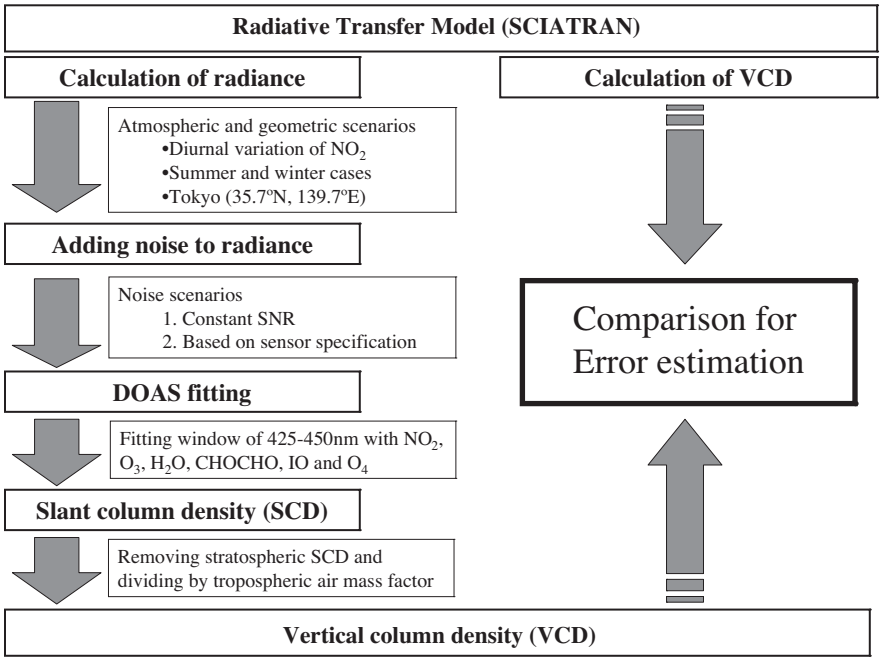

Fig. 1. Flow chart of simulations.

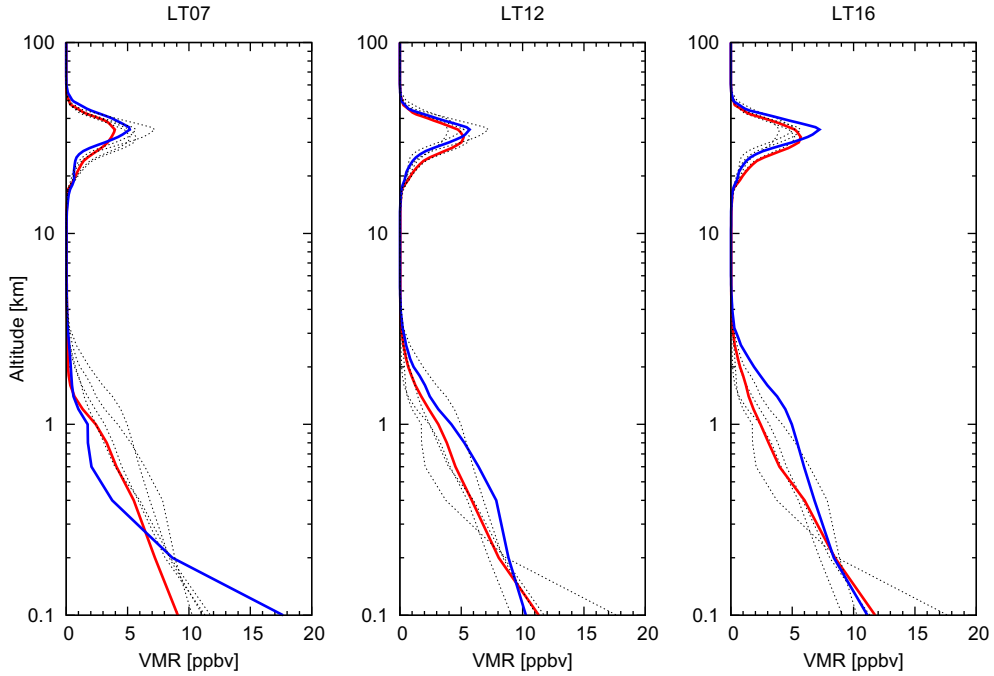

Fig. 2. Vertical profiles of NO_2 used in SCIATRAN for LT07 (left), LT12 (middle) and LT16 (right) in summer (red) and winter (blue). All the panels also include other local times' profiles (shown in broken curves) for comparison.

information on aerosols. We took into account the diurnal and seasonal variations of the stratospheric and the tropospheric NO_2 for typical summer and winter cases by using the results from CTMs. For the stratospheric NO_2, we adopted the results of the Bremen 3D CTM (Sinnhuber et al., 2003a; Sinnhuber et al., 2003b). The Bremen 3D CTM is based on the SLIMCAT model (Chipperfield, 1999) and is a global model with a spatial resolution of 2.5° latitude and 3.75° longitude. The time resolution is 30 minutes. For the tropospheric NO_2, we adopted the results from a CTM based on RAMS (Pielke et al., 1992) and CMAQ (Byun and Schere, 2006). The CTM has a 5 km grid cell for the Tokyo region (200 km × 200 km). The emission inventory used in the CTM includes hourly and monthly emission changes with a 10 km grid cell in the Tokyo region (Kannari et al., 2007). The vertical profiles of gas species except NO_2 were adopted from the database provided by the scientific requirement team in the GMAP-Asia project. The database was developed based on the measurements performed during the TRACE-P aircraft mission (Jacob et al., 2003) and the numerical simulations by the WRF/Chem model version 3.0.1 (Grell et al., 2005) with the calculation conditions defined in Takigawa et al. (2007) and also by the CHASER model (Sudo et al., 2002). For simplicity, we did not take into account seasonal or diurnal variations of those gas species. Pressure and temperature were taken from the US standard atmosphere. The vertical profiles of gas species, temperature and pressure (taking the logarithm) were linearly interpolated with a vertical resolution of 200 m for the altitudes of 0–10 km, 500 m for 10–12 km and 1 km for 12–100 km. Figs. 2 and 3 shows the vertical profiles of NO_2 and other gas species utilized in the radiative transfer calculations in the present study.

For aerosols, we adopted a typical mixing state described in Hess et al. (1998) with the options prepared by SCIATRAN. Table 1 summarizes the details of the aerosol conditions assumed in the present study. We also assume a vertical profile of the extinction coefficient with a scale height of 3 km and an optical depth of 0.2 at a wavelength of 550 nm. The intensity of the radiance simulated by SCIATRAN became 2–5% smaller (depending on wavelength and geometrical conditions) when we included the effect of aerosols.

We did not take into account the effect of clouds in the RT calculation. We discuss the effect of clouds on the GEO measurement in Section 3.4 by using results reported in the literature for OMI measurements.

As an incident solar spectrum, we adopted a solar spectrum derived by Chance and Spurr (1997). The absorption cross sections adopted in the present study are summarized in Table 2. We convoluted the solar spectrum and the absorption cross sections with a Gaussian slit function (FWHM = 0.4 nm) and interpolated them by spline curve with a wavelength grid of 0.1 nm. SCIATRAN can take into account the temperature dependence of absorption cross sections of gases. We conducted simulations for two cases with respect to the temperature dependency; first we neglected the temperature dependence (Section 3.1) and second, we considered the temperature dependence of the cross sections of ozone and NO_2 in Section 3.2, where we will discuss the bias effect caused by this temperature dependence.

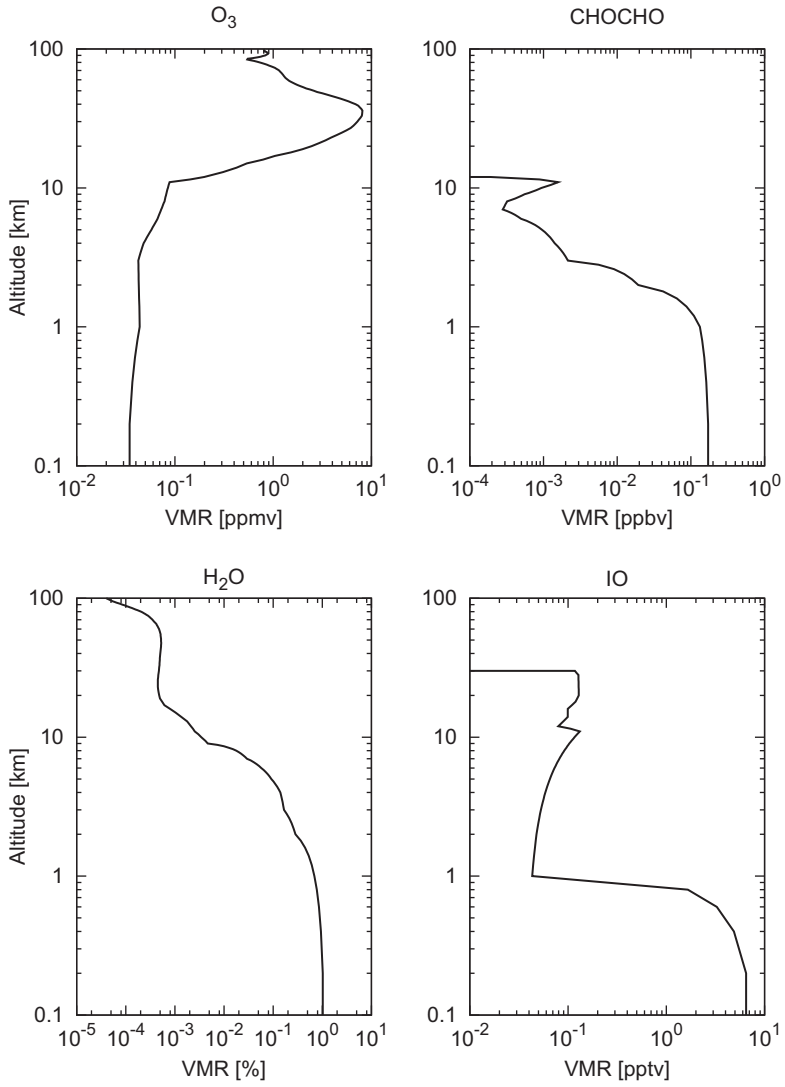

Fig. 3. Vertical profiles of O_3, H_2O, CHOCHO and IO used in SCIATRAN.

Table 1
Aerosol scenario.

Layer Num.	Altitude range	Aerosol types	Components and number mixing ratios	Relative humidity
#1	0–2 km	Urban	Water soluble: 0.177 insoluble: 0.949E−5 soot: 0.823	80%
#2	2–10 km	Continental average	water soluble: 0.458 insoluble: 0.261E−4 soot: 0.542	70%
#3	10–30 km	Sulfate	sulfate: 1	0%
#4	30–100 km	Meteoric	meteoric dust: 1	0%

Table 2
Absorption cross sections used in the present study.

Gas species	Reference
O_3	Voigt et al. (2001)
NO_2	Voigt et al. (2002)
CHOCHO	Volkamer et al. (2005)
IO	Martín et al. (2005)
H_2O	Rothman et al. (2009)
O_4	Greenblatt et al. (1990)

For the definition of the scenario in SCIATRAN, three angles are needed; solar zenith angle (SZA), relative azimuth angle (the angle between the sun and a GEO satellite or an observation point at the ground surface) and line-of-sight (LOS) angle. Fig. 4 summarizes the definitions of those angles in SCIATRAN. We prepared a diurnal variation of SZAs and relative azimuth angles for summer and winter solstices as shown in Table 3. The LOS angle is constant for a geostationary satellite; 46.4° at the surface, and 6.3° at the satellite position, which is chosen to be located at the altitude of 36,000 km over 120°E on the equator.

Data derived from GOME measurements (Koelemeijer et al., 2003) and OMI measurements (Kleipool et al.,

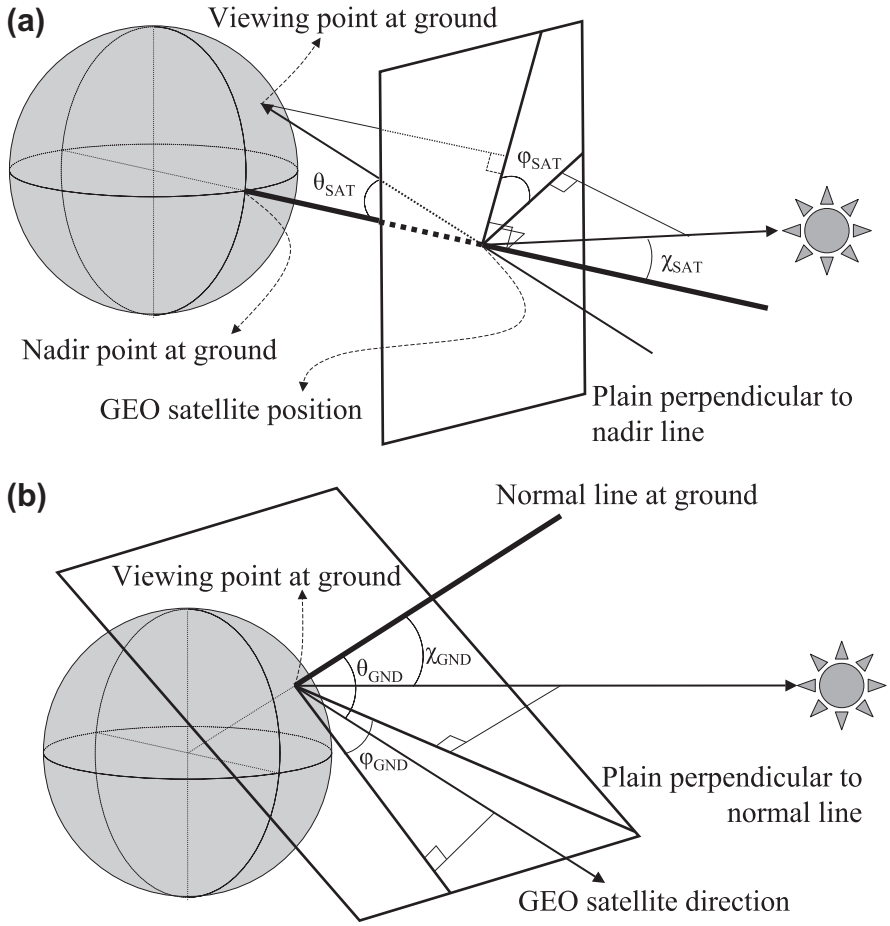

Fig. 4. Definition of the angles used in SCIATRAN (a) for the GEO satellite position and (b) for the viewing point at the ground. χ is solar zenith angle (SZA), θ is line-of-sight (LOS) viewing angle, and φ is relative azimuth angle between the sun and the viewing direction.

Table 3
Geometrical scenario.

LT	GEO (120°E on the equator)				Tokyo (35.7°N, 139.7°E)			
	Summer solstice		Winter solstice		Summer solstice		Winter solstice	
	SZA	RAZ	SZA	RAZ	SZA	RAZ	SZA	RAZ
05	117.6	38.2	116.8	91.4	84.5	146.6	111.0	107.1
06	104.1	40.6	103.2	89.0	73.2	138.7	99.4	99.3
07	90.4	41.4	89.2	88.2	61.4	131.1	88.2	90.9
08	76.6	40.8	75.7	89.0	49.3	123.1	78.5	81.4
09	63.0	38.3	62.1	91.6	37.1	113.7	70.0	70.1
10	49.9	33.6	49.0	96.5	25.4	99.7	63.5	56.9
11	37.7	24.2	36.9	106.2	15.3	71.6	59.8	41.9
12	27.8	6.3	27.3	124.9	12.8	13.4	59.3	25.9
13	23.5	24.2	23.4	156.1	20.7	27.6	62.1	10.5
14	27.5	55.2	27.8	173.4	32.0	45.6	67.8	3.3
15	37.1	73.8	37.6	155.6	44.1	56.4	75.7	15.1
16	49.2	83.3	49.8	146.3	56.2	64.8	85.2	25.2
17	62.3	88.4	63.1	141.5	68.2	72.4	96.0	33.9
18	75.9	90.9	76.7	139.2	79.8	80.1	107.4	41.8
19	89.2	91.3	90.5	138.5	90.2	88.5	119.3	49.4

LT: local time at Tokyo, SZA: solar zenith angle, RAZ: relative azimuth angle. Satellite's zenith angle and azimuth angle at Tokyo are 46.4° and 211.5°, respectively.

2008) show that the Lambert Equivalent Reflectance over Tokyo is 0.04 and 0.06–0.07, respectively. In the present study, we assumed a surface albedo of 0.05 in all the radiative transfer calculations except in Section 3.3, where we assumed a different surface albedo to examine the effect of albedo uncertainty on the retrieval precision.

2.2. Consideration of sensor noise

In the present study, we prepared two scenarios for sensor noise. One is very simple and general; we just assume a constant SNR of 100, 200, 500, 1000, 2000 and 5000. The other scenario is more realistic; we take into account the sensor specification, which is discussed in the GMAP-Asia project. We assume a back-illuminated scanning CCD as a detector, and we can generally define SNR η as follows (Yamamoto, 2008, private communication):

$$\eta = \frac{S}{\sqrt{S + N_{read}^2}} \tag{1}$$

where

$S = (R \cdot \pi D^2/4 \cdot \Omega \cdot \Delta\lambda \cdot \tau \cdot \Delta\ t \cdot \varepsilon) \cdot \lambda/hc$
S: signal electron number [e]
N_{read}: reading noise (= 20 [e])
R: radiance [W m^{-2} sr^{-1} nm^{-1}]
D: aperture diameter (= 9.0×10^{-2}[m])
Ω: solid angle (= 7.72×10^{-8} [sr])
$\Delta\lambda$: sampling width (= 4.0×10^{-1} [nm])
(we assume that the sampling width is equal to the FWHM in this definition)
τ: optical efficiency (= 0.1)
Δt: the time assigned for each step's spatial scanning time (= 1.25 [s])
ε: detector efficiency (= 0.5)
λ: wavelength [m]
h: Planck's constant [J s]
c: velocity of light [m s^{-1}]

In this definition, shot noise and reading noise of the CCD detector are included. As the SNR depends on the intensity of the input signal (i.e., radiance), the SNR depends also on season and local time.

Note that the exact sensor specification has not yet been decided in the project, and here we assume plausible numbers, which are listed in parentheses in the definition mentioned above. Those numbers are based on Yamamoto [2008, private communication] and are currently discussed in the project. We also assume that the sensor has an instantaneous field of view (IFOV) of 10 km in an observation domain of 4000 km × 4000 km and a sampling time of 1 h.

By using Eq. (1), we calculated the magnitudes of the SNR at each wavelength step for a given radiance calculated by SCIATRAN. Then, we calculated the noise components according to the magnitude of the SNR using random numbers generated by the Mersenne twister algorithm (Matsumoto and Nishimura, 1998). Finally, we added the noise components to the original radiance spectrum and regarded the radiance spectrum including the noise components as a final product of the Earth's atmospheric spectrum. We prepared one hundred spectra according to one hundred seeds of random numbers for a single set of the parameters (season, local time, and SNR) to estimate the NO_2 errors statistically.

2.3. DOAS fitting and conversion of SCDs into VCDs

To derive the SCDs of NO_2 from the synthesized Earth's atmospheric spectra, we applied differential optical absorption spectroscopy (DOAS) (Platt, 1994). DOAS is a proven method to retrieve weakly absorbing atmospheric constituents from space-borne measurements. The DOAS method obtains the SCDs of the gas species present along the ray's path, solving a simultaneous equation system including the relationship between the absorption cross sections of the supposed gases and the observed spectrum with linear/non-linear fitting. The details of the application of DOAS to satellite measurements are described in the existing literature (e.g. Burrows et al., 1999; Bovensmann et al., 1999). In the present study, we used a fitting window between 425–450 nm and took into account not only NO_2, but also O_3, H_2O, CHOCHO, IO and O_4, which all have absorption features in the fitting window. A third order polynomial was used in the fit. The simulations did not include rotational Raman scattering that leads to the filling in of Fraunhofer lines. For each set of the parameters, one hundred SCDs were obtained by DOAS as one hundred spectra were calculated.

The NO_2 SCDs obtained from the DOAS fitting are the total NO_2 SCDs including the stratospheric NO_2 SCDs and the tropospheric NO_2 SCDs. In the present study, we converted the total NO_2 SCDs into the tropospheric NO_2 VCDs as follows:

$$\mathrm{VCD}_{trop}^{DOAS} = (\mathrm{SCD}_{total}^{DOAS} - \mathrm{SCD}_{strat}^{RTM})/\mathrm{AMF}_{trop}^{RTM} \tag{2}$$

where $\mathrm{VCD}_{trop}^{DOAS}$ is a tropospheric VCD, $\mathrm{SCD}_{total}^{DOAS}$ is a total (tropospheric and stratospheric) SCD retrieved by DOAS, $\mathrm{SCD}_{strat}^{RTM}$ is a stratospheric SCD calculated by a RTM (SCIATRAN) and $\mathrm{AMF}_{trop}^{RTM}$ is a tropospheric air mass factor (AMF) calculated by a RTM (SCIATRAN) at 437 nm, which is the approximate center wavelength of the DOAS fitting window (425–450 nm). Fig. 5 shows the diurnal variations of the stratospheric and tropospheric NO_2 VCDs, SCDs and AMFs, all of which are calculated by SCIATRAN under summer and winter conditions, respectively. The $\mathrm{SCD}_{strat}^{RTM}$ in Eq. (2) are shown as thin curves in Fig. 5 (a) and the $\mathrm{AMF}_{trop}^{RTM}$ are shown as broken curves in Fig. 5 (b). In this conversion, we neglect uncertainties in the determination of the stratospheric SCD and the tropospheric AMF. Although these two errors are critical in real measurements (Boersma et al., 2004), the investigation of the effect of these errors on GEO measurements is out of the scope in the present study. Then, we finally calculated standard deviations and averages of the retrieved NO_2 VCDs. We interpret the standard deviation as an estimate of the precision.

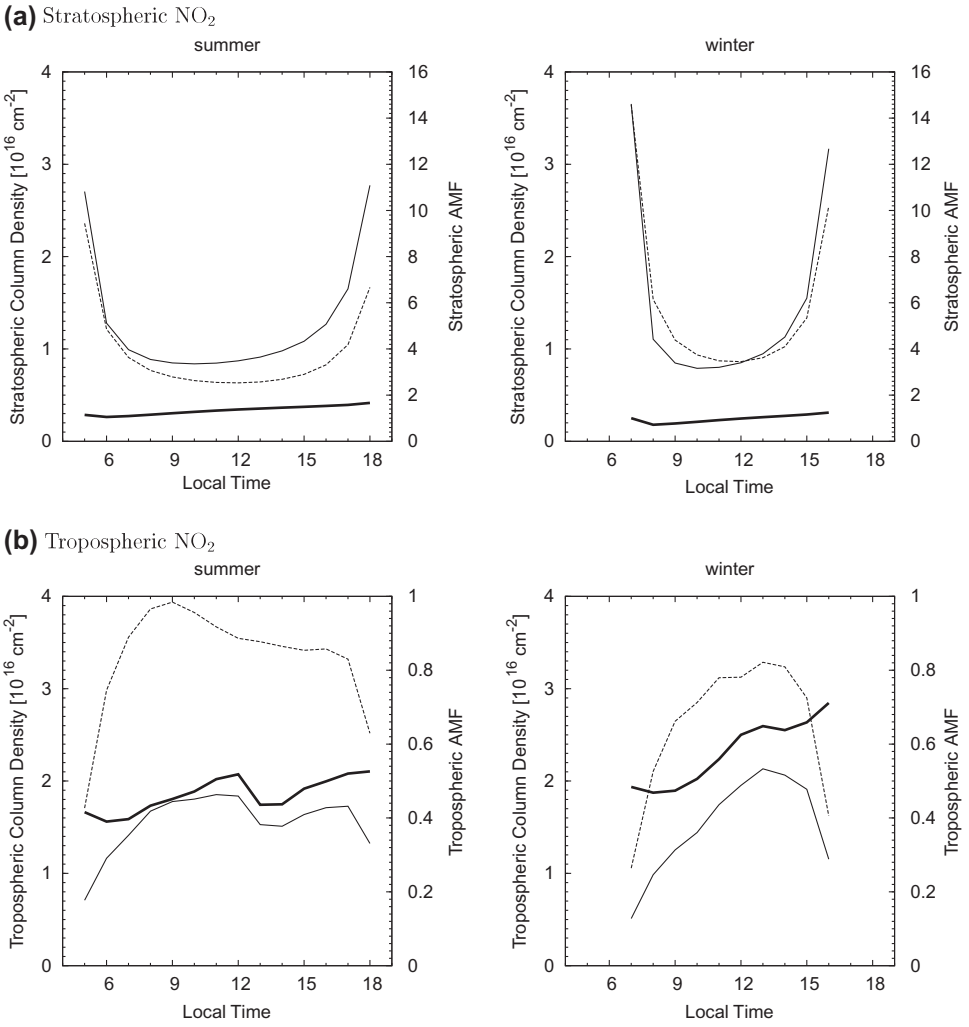

Fig. 5. Vertical column density (VCD, thick curve), slant column density (SCD, thin curve) and air mass factor (AMF, broken curve) of NO_2 (a) for the stratosphere and (b) for the troposphere calculated by SCIATRAN. SCD and AMF are calculated at the wavelength of 437 nm. Note that the *y*-axis scales for the AMFs are different in panels (a) and (b).

2.4. Diurnal variations of VCDs, SCDs and AMFs

Before proceeding to the error estimation of the tropospheric NO_2 VCDs, we briefly investigate the basic behavior of the diurnal variations of NO_2 VCDs, SCDs and AMFs for a GEO measurement (Fig. 5).

Several effects contribute to the importance of the stratospheric NO_2: The relative size of the NO_2 amounts in the stratosphere and troposphere, their change over the day and the difference in sensitivity of the measurements for the two regions, expressed as AMF. The variation in stratospheric SCDs depends strongly on solar zenith angle and is almost entirely caused by the change in stratospheric AMFs, which can be approximated by the geometric AMF, $1/\cos(\mathrm{LOS}) + 1/\cos(\mathrm{SZA})$. The tropospheric AMF in contrast changes much less over the day, and has a minimum at large SZAs.

According to the CTMs utilized in the present study, the tropospheric VCDs (order of $10^{16}\,\mathrm{cm}^{-2}$) are much larger than the stratospheric VCDs (order of $10^{15}\,\mathrm{cm}^{-2}$), and have larger diurnal variations. This means that much more NO_2 exists in the troposphere than in the stratosphere over Tokyo. However, the SCDs, which are directly obtained from the measurements, behave differently; the stratospheric SCDs are comparable to the tropospheric SCDs. Therefore, the relatively small amount of the stratospheric NO_2 could still significantly affect the measurements of the total SCDs. This is due to the magnitude of the AMFs; the tropospheric AMFs (<1) are much smaller than the stratospheric AMFs (4–15). In particular, the difference between the tropospheric and stratospheric AMFs becomes larger in the morning and evening than during daytime, and then the stratospheric SCDs overtake the tropospheric SCDs in the morning and evening. The stratospheric SCDs also change very rapidly in the morning and evening. Therefore, the measurements in the morning and evening could be more strongly affected by the stratosphere than during daytime.

One fact could improve the measurement in the morning and evening; the diurnal variations of the stratospheric

VCDs are small in the morning and evening compared to the diurnal variations of the stratospheric AMFs as mentioned above. For example, the stratospheric VCD decreases by 8% from LT05 to LT06 in summer, while the stratospheric AMF decreases nearly by 50%. Consequently, the apparent variations of the stratospheric SCDs in the morning and evening are primarily caused by the change in stratospheric AMFs. As the diurnal variation of the SZA can be calculated with high accuracy, the relative variation of the stratospheric SCDs can be well estimated. During the daytime, in contrast, the diurnal variation of the stratospheric VCD becomes more important for the diurnal variation of the stratospheric SCDs.

Fig. 5 also indicates that the tropospheric AMFs become smaller (half or less) in the morning and evening than during daytime. This means that the sensitivity for the tropospheric NO_2 decreases in the morning and evening even if the stratospheric NO_2 is fully accounted for. On the other hand, the stratospheric AMFs behave vice versa; the sensitivity for the stratospheric NO_2 increases in the morning and evening.

3. Results

3.1. Precision of the tropospheric VCDs

The diurnal variation of the retrieved tropospheric NO_2 VCDs and the derived precisions are shown in Fig. 6. In summer, the minimum and maximum of the diurnal variation of the tropospheric VCDs occurs at LT06 and LT12/18, respectively. The magnitude of the diurnal variations is 0.5×10^{16} cm^{-2}, which requires at least a SNR of 500 to be detected. A SNR $\geqslant$ 1000 is needed to observe the local minimum occurring in the early afternoon (LT13–14). In winter, the diurnal variation of the tropospheric VCDs has a magnitude of 1×10^{16} cm^{-2} from morning to evening. The detection of the diurnal variation during LT08–15 needs SNR $\geqslant$ 500, and SNR $\geqslant$ 1000 is needed if early morning (LT07) and early evening (LT16) are included. As shown in Fig. 5, the precisions in the morning and evening become worse because of the smaller tropospheric AMFs.

The relative values of the precision are shown in Fig. 7. For GMAP-Asia, a value of 10–30% of the VCD was proposed as the target measurement precision for tropospheric NO_2 (Akimoto et al., 2008). The precision of 30% and 10% is almost achieved by SNR $\geqslant$ 200 and SNR $\geqslant$ 500, respectively, except in the morning and evening. A SNR $\geqslant$ 1000 or even 2000 is required to achieve the precision of 10% if morning and evening observations are included.

The assumed sensor, which has a horizontal resolution of 10 km and a temporal resolution of 1hr, has a precision of several percent, which is approximately corresponding to a SNR = 1000–2000, except in the morning and evening. Even in the morning and evening, the precision is corresponding to a SNR = 500 (in the winter early morning) or better. Therefore, the assumed sensor is able to detect the diurnal variation of the tropospheric NO_2 simulated in the present study except in the winter early morning, and is mostly able to fulfill the requirement of the proposal by the GMAP-Asia project for the observations over Tokyo.

Single measurements are accurate enough to observe a diurnal cycle at strongly polluted sites such as Tokyo. For areas with lower signals, spatial averaging would be needed. For example, our additional simulations indicate that a binning over four CCD pixels corresponding to ground pixels of 20 km $\times$ 20 km or 400 km^2 would result in a 40% decrease of the VC error, enabling diurnal variations of 0.3×10^{16} (in summer) and 0.6×10^{16} (in winter) [molec cm^{-2}] to be detected if a pattern of the diurnal variation similar to that in Tokyo were assumed. Not only spatial averaging but also temporal (monthly/seasonal) averaging will contribute to improving the precision of diurnal patterns of NO_2.

The results mentioned above could be (partially) applied to other geostationary satellites. Sentinel 4 UVN, for example, is planned to provide a spatial (8 km $\times$ 8 km) and temporal (1 h) resolution (Bovensmann et al., 2010) which is similar to the resolution of the planned GMAP-Asia sensor. If the amounts of NO_2 and other factors (aerosols etc.) over Europe are also similar, observations of diurnal variations in the tropospheric NO_2 in that area will be possible with that instrument as well.

3.2. Effect of temperature dependence of absorption cross section

For simplicity, no temperature dependency of the absorption cross sections was considered in the radiative transfer calculations shown in Figs. 6 and 7, where we used the NO_2 absorption cross section for a single temperature (223 K) in the radiative transfer calculation, and also used the same cross section in the DOAS fitting. In the real atmosphere, however, the absorption cross section depends on atmospheric temperature and this should be taken into account in the retrieval. The problem is that the DOAS analysis utilizes absorption cross sections for individual temperatures. Fig. 8 shows the biases which are caused by the use of an absorption cross section at inappropriate temperatures in the DOAS analyses. In this figure, the radiative transfer calculation took into account the temperature dependency of the absorption cross sections of NO_2 and O_3 in the troposphere and stratosphere, but a single temperature's absorption cross section was utilized in the DOAS analysis. The absorption cross section at 280 K gives the best results during the daytime among the temperatures drawn in Fig. 8, but in the morning and evening, the cross section at 280 K causes large biases (0.5–1×10^{16} cm^{-2}) and the use of the cross section at colder temperature (260 K) results in better accuracy. During the daytime, inappropriate temperature would cause a systematic error of 0.1–1%/K, depending on local time and season. Boersma et al. (2004) estimated the systematic

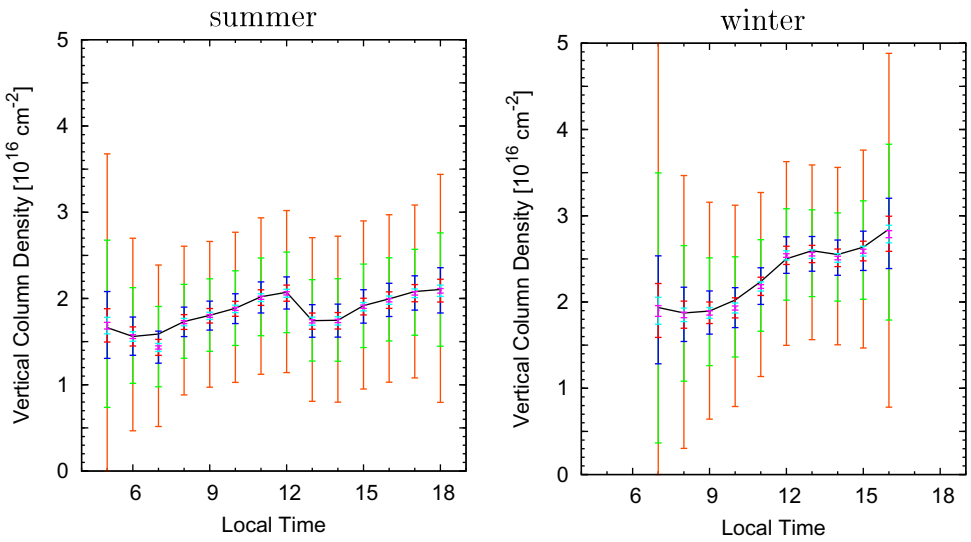

Fig. 6. Vertical column density (VCD) of NO_2 derived by DOAS with precision (standard deviation) for SNR = 100 (orange), SNR = 200 (green), SNR = 500 (dark blue), SNR = 1000 (red), SNR = 2000 (light blue), and SNR = 5000 (pink). VCD calculated by SCIATRAN is also shown (black curve).

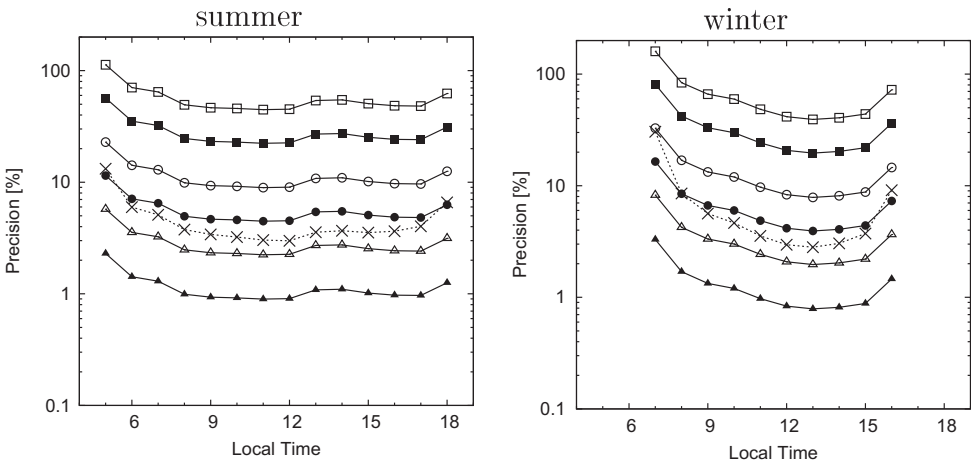

Fig. 7. Precision (standard deviation) of vertical column density (VCD) of NO_2 derived by DOAS for SNR = 100 (outline square), SNR = 200 (solid square), SNR = 500 (outline circle), SNR = 1000 (solid circle), SNR = 2000 (outline triangle), and SNR = 5000 (solid triangle). Precision for the assumed sensor with a horizontal resolution of 10 km and a time resolution of 1 h is also shown (broken curve with crosses). We assumed that surface albedo is 0.05.

effect of not accounting for atmospheric temperature variations as −5% to −7% for SCDs around Tokyo when they used an absorption cross section taken at 221 K for the GOME retrieval and did not apply any correction for the SCDs. Our estimation gives comparable values: −9% to −10% for the SCD's errors, which are estimated as the difference of the SCDs fitted by using the absorption cross sections of 223 K and 280 K.

The effective temperature of NO_2, which we define here as the temperature which gives the best fit in the DOAS analysis, is generally determined by the relative profiles of the box AMFs (that are dependent of SZA amongst other variables), the NO_2 profile, and the temperature profile. Although the vertical distribution of NO_2 and temperature could affect the effective temperature, the lowering of the effective temperature shown in Fig. 8 is primarily attributed to the diurnal variation of the box AMFs (SZA). In the morning and evening the SZA is large, and the light path becomes longer in the stratosphere, where the atmospheric temperature is colder than in the troposphere. Therefore, the absorption cross section at the lower temperature gives better agreement in the morning and evening.

In the practical retrievals of the tropospheric NO_2 by the existing LEO satellites, an empirical correction for the temperature dependence of the absorption cross section is performed (Boersma et al., 2004). The GEO measurements

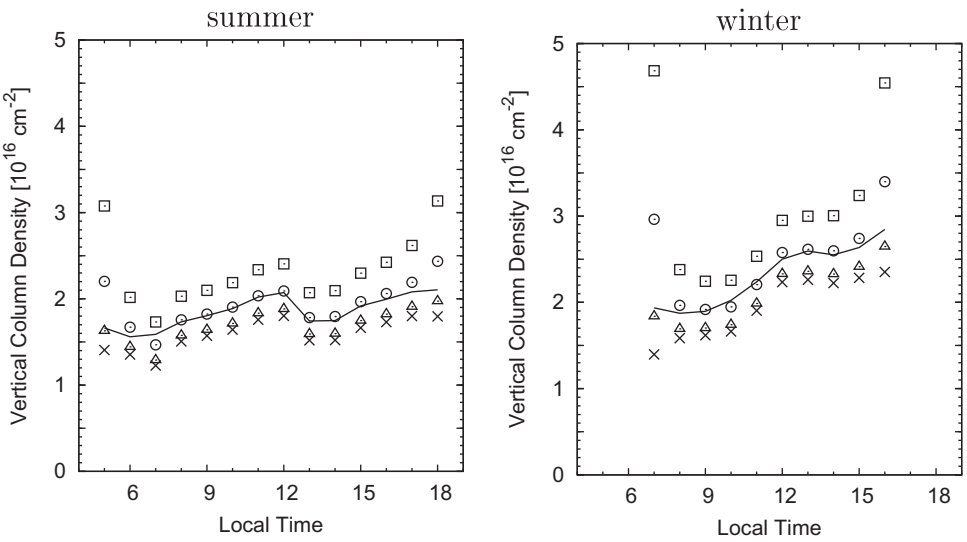

Fig. 8. Vertical column density (VCD) of NO_2 derived by DOAS using the NO_2 absorption cross section for 223 K (cross), 260 K (outline triangle), 280 K (outline circle) and 293 K (outline square). No noise is taken into account. VCD calculated by SCIATRAN is also shown (black curve).

would also need such a correction for the temperature dependence of absorption cross section, depending on season and local time.

3.3. Effect of surface spectral reflectance

The uncertainty of the surface spectral reflectance also affects the precision of the tropospheric NO_2 retrieval. Typical albedos for soils, forests, and urban areas range from ~0.05 to 0.2 (Schanda, 1986). Fig. 9 shows the relative precision of the retrievals as Fig. 7, but for a surface albedo of 0.20. When the albedo changes from 0.05 to 0.20, the precision improves by a factor of two (i.e., the error is reduced by half). If there is a high variability of albedo at the surface, the precision expected will also vary largely. At the same time, the surface albedo also has a large impact on the sensitivity to tropospheric NO_2 which has to be taken into account. The evaluation of the albedo in the region focused on will be important for the accuracy of the retrieval and a proper error estimation.

3.4. Effect of clouds

In the discussion above, we neglected the effect of clouds and supposed only clear-sky conditions. In the real measurements, however, clouds come into the field of view of sensors. In this section, we briefly discuss the effect of clouds on the GEO measurements of the diurnal variation of the tropospheric NO_2.

The main effects of clouds on the tropospheric NO_2 retrieval are caused by uncertainties in the determination of cloud fraction and cloud height (Boersma et al., 2004). We suppose that the two cloud parameters can be retrieved simultaneously in the retrieval of the tropospheric NO_2. Boersma et al. (2007) conducted the retrieval of the cloud parameters for the retrieval of the tropospheric NO_2 by

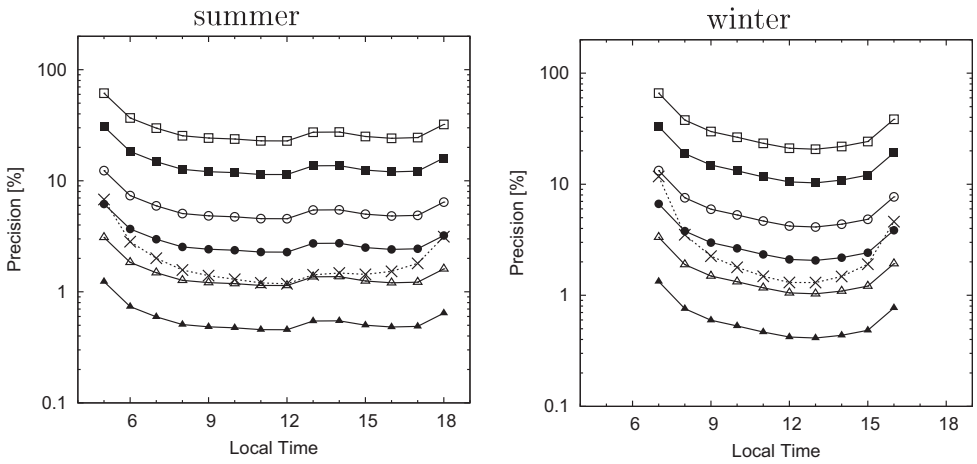

Fig. 9. Same as Fig. 7, but for surface albedo of 0.20.

using the visible channel including the O_2—O_2 absorption structure at 477 nm by OMI. The authors estimated the errors of cloud fraction and cloud height as 0.05 and 60hPa, respectively, and the errors result in tropospheric AMF errors (i.e., the VCD errors) of 30% and 15 %, respectively. If we assume the same magnitude of the errors in the GEO measurements, the magnitude of the error is larger than the precision required for the detection of the diurnal variation of the tropospheric NO_2. Therefore, averaging or strict data selection will be needed to reduce the errors due to clouds.

In the GEO measurements, however, the pixel size at the surface ground is smaller than for existing measurements. Therefore, as an increased number of cloud free observations is expected at the better spatial resolution of the instrument (Krijger et al., 2007), the errors expected should be less critical than estimated above. We should also consider the possibility that cloud properties could have systematic diurnal cycles which could cause artificial patterns in the NO_2 field.

4. Conclusions and future tasks

The present study investigates the minimum SNR of a GEO sensor required to detect the diurnal variation of the tropospheric NO_2 over Tokyo by using numerical simulations. In summer, a SNR $\geqslant$ 500 is needed to detect the diurnal variations and a SNR $\geqslant$ 1000 is needed to observe the local minimum occurring in the early afternoon (LT13–14). In winter, the detection of the diurnal variation during LT08–15 requires a SNR $\geqslant$ 500, and a SNR $\geqslant$ 1000 is needed if early morning (LT07) and early evening (LT16) are included. The currently discussed sensor specification for GMAP-Asia, which has a horizontal resolution of 10 km and a time resolution of 1 h, has demonstrated the performance of a precision of several percent, which is approximately corresponding to SNR = 1000–2000 during daytime and SNR $\geqslant$ 500 in the morning and evening. The proposed sensor is therefore able to detect the diurnal variation of the tropospheric NO_2 simulated in the present study except in the winter early morning, and is mostly able to fulfill the requirements made in the proposal for the GMAP-Asia project for the observations over Tokyo. We also discussed the possible biases caused by the temperature dependence of the absorption cross section utilized in the DOAS retrieval and the effect of uncertainties of surface albedo and clouds on the estimation of precisions.

For the future, it is very important to perform more detailed error estimates not only for the retrieval of SCDs, but also for the removal of the stratospheric component and the evaluation of the tropospheric air mass factor, which have been discussed for the existing LEO measurements of tropospheric NO_2 (Boersma et al., 2004). One of the problems to be solved is the dependence of surface spectral reflectance on SZA in the AMF estimation. In the LEO measurements, the SZA is almost constant but the LOS angle is variable, and the surface spectral reflectance depends on the LOS angle. Recently, it has been shown that the dependence of surface albedo on the LOS angle affects the AMF estimation in tropospheric NO_2 measurements (Zhou et al., 2010). In the GEO measurement, the situation is vice versa; the LOS angle is constant but the SZA is variable. It would also be important to evaluate the dependence of surface albedo on SZA in the AMF estimations for GEO measurements, as the SZA changes over the course of a day and it can greatly influence the observed diurnal NO_2 pattern.

Acknowledgements

We would like to thank Hajime Akimoto, Yasuko Kasai, Kazuyuki Kita and other members of the GMAP-Asia project and the Japan Society of Atmospheric Chemistry. We are deeply grateful to Alexei Rozanov of IUP/Bremen for providing SCIATRAN. We would like to thank Yasuji Yamamoto of JAXA for the discussion of SNR. The C library of Mersenne Twister algorithm was provided by the following website: http://www.math.sci.hiroshima-u.ac.jp/m-mat/MT/emt.html. For the calculation of the SZA and LOS angles, we utilized the website of the National Astronomical Observatory of Japan (http://www.nao.ac.jp/koyomi/koyomix/koyomix.html). K. Noguchi was supported by JSPS Postdoctoral Fellowships for Research Abroad during the research stay at the Institute of Environmental Physics, University of Bremen, Germany. A. Hilboll would like to thank the Helmholtz Gemeinschaft's Earth System Science Research School (ESSReS) for funding his Ph.D. work. Financial support by the European Union through the CITYZEN project (Grant No. 212095) is gratefully acknowledged.

References

Akimoto, H., Kasai, Y., Kita, K. (Eds.). Planning a Geostationary Atmospheric Observation Satellite. National Institute of Information and Communications Technology, 2008.

Akimoto, H., Kasai, Y., Kita, K., Irie, H., Sagi, K., Hayashida, S. Geostationary atmospheric observation satellite plan in Japan (Invited). AGU Fall Meeting Abstracts. A51M–01, 2009.

Boersma, K.F., Eskes, H.J., Brinksma, E.J. Error analysis for tropospheric NO_2 retrieval from space. J. Geophys. Res. 109, D04311, doi:10.1029/2003JD003962, 2004.

Boersma, K.F., Eskes, H.J., Veefkind, J.P., Brinksma, E.J., van der A, R.J., Sneep, M., van den Oord, G.H.J., Levelt, P.F., Stammes, P., Gleason, J.F., Bucsela, E.J. Near-real time retrieval of tropospheric NO_2 from OMI. Atmos. Chem. Phys. 7, 2103–2118, 2007.

Boersma, K.F., Jacob, D.J., Eskes, H.J., Pinder, R.W., Wang, J., van der A, R.J. Intercomparison of SCIAMACHY and OMI tropospheric NO_2 columns: Observing the diurnal evolution of chemistry and emissions from space. J. Geophys. Res. 113, D16S26, doi:10.1029/2007JD008816, 2008.

Boersma, K.F., Jacob, D.J., Trainic, M., Rudich, Y., Desmedt, I., Dirksen, R., Eskes, H.J. Validation of urban NO_2 concentrations and their diurnal and seasonal variations observed from the SCIAMACHY and OMI sensors using in situ surface measurements in Israeli cities. Atmos. Chem. Phys. 9, 3867–3879, 2009.

Bovensmann, H., Burrows, J.P., Buchwitz, M., Frerick, J., Noël, S., Rozanov, V.V., Chance, K.V., Goede, A.P.H. SCIAMACHY: mission

objectives and measurement modes. J. Atmos. Sci. 56, 127–150, doi:10.1175/1520-0469(1999)056<0127:SMOAMM>2.0.CO;2, 1999.

Bovensmann, H., Noël, S., Bramstedt, K., Liebing P., Richter, A., Rozanov, V., Vountas, M., Burrows, J.P., Veihelmann, B. Sentinel 4 UVN on Meteosat third generation: expected product quality, in: 38th COSPAR Scientific Assembly, A11–0010–10, 2010.

Bovensmann, H., Noël, S., Monks, P., Goede, A.P.H., Burrows, J.P. The geostationary scanning imaging absorption spectrometer (GeoSCIA) mission: requirements and capabilities. Adv. Space Res. 29, 1849–1859, doi:10.1016/S0273-1177(02)00104-7, 2002.

Burrows, J.P., Bovensmann, H., Bergametti, G., Flaud, J.M., Orphal, J., Noël, S., Monks, P.S., Corlett, G.K., Goede, A.P., von Clarmann, T., Steck, T., Fischer, H., Friedl-Vallon, F. The geostationary tropospheric pollution explorer (GeoTROPE) mission: objectives, requirements and mission concept. Adv. Space Res. 34, 682–687, doi:10.1016/j.asr.2003.08.067, 2004.

Burrows, J.P., Weber, M., Buchwitz, M., Rozanov, V., Ladstätter-Weißenmayer, A., Richter, A., Debeek, R., Hoogen, R., Bramstedt, K., Eichmann, K.U., Eisinger, M., Perner, D. The global ozone monitoring experiment (GOME): mission concept and first scientific results. J. Atmos. Sci. 56, 151–175, doi:10.1175/1520-0469(1999)056, 1999.

Byun, D., Schere, K.L. Review of the governing equations, computational algorithms, and other components of the models-3 community multiscale air quality (CMAQ) modeling system. Appl. Mech. Rev. 59, 51–77, doi:10.1115/1.2128636, 2006.

Callies, J., Corpaccioli, E., Eisinger, M., Hahne, A., Lefebvre, A. GOME-2 Metop's second-generation sensor for operational ozone monitoring. ESA Bull. 102, 28–36, 2000.

Chance, K.V., Spurr, R.J.D. Ring effect studies: Rayleigh scattering, including molecular parameters for rotational raman scattering, and the fraunhofer spectrum. Appl. Opt. 36, 5224–5230, 1997.

Chipperfield, M.P. Multiannual simulations with a three-dimensional chemical transport model. J. Geophys. Res. 104, 1781–1806, doi:10.1029/98JD02597, 1999.

Edwards, D.P. Air quality remote sensing from space. Trans. Am. Geophys. Union (EOS) 87, doi:10.1029/2006EO330005, 2006.

Greenblatt, G.D., Orlando, J.J., Burkholder, J.B., Ravishankara, A.R. Absorption measurements of oxygen between 330 and 1140 nm. J. Geophys. Res. 95, 18577–18582, doi:10.1029/JD095iD11p18577, 1990.

Grell, G.A., Peckham, S.E., Schmitz, R., McKeen, S.A., Frost, G., Skamarock, W.C., Eder, B. Fully coupled "online" chemistry within the WRF model. Atmos. Environ. 39, 6957–6975, doi:10.1016/j.atmosenv.2005.04.027, 2005.

Hess, M., Koepke, P., Schult, I. Optical properties of aerosols and clouds: the software package OPAC. Bull. Amer. Meteorol. Soc. 79, 831–844, doi:10.1175/1520-0477(1998)079<0831:OPOAAC>2.0.CO;2, 1998.

Hobbs, P.V. Introduction to Atmospheric Chemistry. Cambridge University Press, 2000.

Irie, H., Iwabuchi, H., Kasai, Y., Kita, K., Akimoto, H. A simulation for UV–VIS observations of tropospheric composition from a GEO satellite over Asia. AGU Fall Meeting Abstracts. A53A-0244, 2009.

Jacob, D.J., Crawford, J.H., Kleb, M.M., Connors, V.S., Bendura, R.J., Raper, J.L., Sachse, G.W., Gille, J.C., Emmons, L., Heald, C.L. Transport and chemical evolution over the pacific (TRACE-P) aircraft mission: design, execution, and first results. J. Geophys. Res. 108, 9000, doi:10.1029/2002JD003276, 2003.

Kannari, A., Tonooka, Y., Baba, T., Murano, K. Development of multiple-species resolution hourly basis emissions inventory for Japan. Atmos. Environ. 41, 3428–3439, doi:10.1016/j.atmosenv.2006.12.015, 2007.

Kelder, H., Van Weele, M., Goede, A., Kerridge, B.J., Reburn, J., Bovensmann, H., Monks, P., Remedios, J., Mager, R., Sassier, H., Baillon, Y. Operational Atmospheric Chemistry Monitoring Missions: CAPACITY - Composition of the Atmosphere: Progress to Applications in the user CommunITY: Final Report, volume 17237/03/NL/GS. European Space Agency, 2005.

Kim, S., Heckel, A., Frost, G.J., Richter, A., Gleason, J., Burrows, J.P., McKeen, S., Hsie, E., Granier, C., Trainer, M. NO_2 columns in the western United States observed from space and simulated by a regional chemistry model and their implications for NO_x emissions. J. Geophys. Res. 114, D11301, doi:10.1029/2008JD011343, 2009.

Kleipool, Q.L., Dobber, M.R., de Haan, J.F., Levelt, P.F. Earth surface reflectance climatology from 3 years of OMI data. J. Geophys. Res. 113, D18308, doi:10.1029/2008JD010290, 2008.

Koelemeijer, R.B.A., de Haan, J.F., Stammes, P. A database of spectral surface reflectivity in the range 335–772 nm derived from 5.5 years of GOME observations. J. Geophys. Res. 108 (4070), doi:10.1029/2002JD002429, 2003.

Krijger, J.M., van Weele, M., Aben, I., Frey, R. Technical Note: the effect of sensor resolution on the number of cloud-free observations from space. Atmos. Chem. Phys. 7, 2881–2891, 2007.

Leue, C., Wenig, M., Wagner, T., Klimm, O., Platt, U., Jähne, B. Quantitative analysis of NO_x emissions from global ozone monitoring experiment satellite image sequences. J. Geophys. Res. 106, 5493–5506, doi:10.1029/2000JD900572, 2001.

Levelt, P.F., van den Oord, G.H.J., Dobber, M.R., Malkki, A., Visser, H., de Vries, J., Stammes, P., Lundell, J.O.V., Saari, H. The ozone monitoring instrument. IEEE Trans. Geosci. Remote Sens. 44, 1093–1101, doi:10.1109/TGRS.2006.872333, 2006.

Little, A.D., Neil, D.O., Sachse, G.W., Fishman, J., Krueger, A.J. Remote sensing from geostationary orbit: GEO TROPSAT, a new concept for atmospheric remote sensing, in: H. Fujisada (Ed.), Society of Photo-Optical Instrumentation Engineers (SPIE) Conference Series, pp. 480–488, 1997.

Martín, J.C.G., Spietz, P., Burrows, J.P. Spectroscopic studies of the I_2/O_3 photochemistry: Part 1: Determination of the absolute absorption cross sections of iodine oxides of atmospheric relevance. J. Photochem. Photobiol. A: Chem. 176, 15–38, doi:10.1016/j.jphotochem.2005.09.024, 2005.

Martin, R.V., Jacob, D.J., Chance, K., Kurosu, T.P., Palmer, P.I., Evans, M.J. Global inventory of nitrogen oxide emissions constrained by space-based observations of NO_2 columns. J. Geophys. Res. 108, 4537, doi:10.1029/2003JD003453, 2003.

Matsumoto, M., Nishimura, T. Mersenne twister: a 623-dimensionally equidistributed uniform pseudo–random number generator. ACM Trans. Model. Comput. Simul. 8, 3–30, doi:10.1145/272991.272995, 1998.

Mijling, B., van der A, R.J., Boersma, K.F., Van Roozendael, M., De Smedt, I., Kelder, H.M. Reductions of NO_2 detected from space during the 2008 Beijing olympic games. Geophys. Res. Lett. 36, 13801, doi:10.1029/2009GL038943, 2009.

Pielke, R.A., Cotton, W.R., Walko, R.L., Tremback, C.J., Lyons, W.A., Grasso, L.D., Nicholls, M.E., Moran, M.D., Wesley, D.A., Lee, T.J., Copeland, J.H. A comprehensive meteorological modeling system–RAMS. Meteorol. Atmos. Phys. 49, 69–91, doi:10.1007/BF01025401, 1992.

Platt, U. Differential optical absorption spectroscopy (DOAS), air monitoring by spectroscopic techniques. Chem. Anal. Ser. 127, 27–84, 1994.

Richter, A., Burrows, J.P., Nüß, H., Granier, C., Niemeier, U. Increase in tropospheric nitrogen dioxide over China observed from space. Nature 437, 129–132, doi:10.1038/nature04092, 2005.

Rothman, L., Gordon, I., Barbe, A., Benner, D., Bernath, P., Birk, M., Boudon, V., Brown, L., Campargue, A., Champion, J.P., Chance, K., Coudert, L., Dana, V., Devi, V., Fally, S., Flaud, J.M., Gamache, R., Goldman, A., Jacquemart, D., Kleiner, I., Lacome, N., Lafferty, W., Mandin, J.Y., Massie, S., Mikhailenko, S., Miller, C., Moazzen-Ahmadi, N., Naumenko, O., Nikitin, A., Orphal, J., Perevalov, V., Perrin, A., Predoi-Cross, A., Rinsland, C., Rotger, M., Simecková, M., Smith, M., Sung, K., Tashkun, S., Tennyson, J., Toth, R., Vandaele, A., Auwera, J.V. The HITRAN 2008 molecular spectroscopic database. J. Quant. Spectr. Rad. Trans. 110, 533–572, doi:10.1016/j.jqsrt.2009.02.013, 2009.

Rozanov, A., Rozanov, V., Buchwitz, M., Kokhanovsky, A., Burrows, J.P. SCIATRAN 2.0 – A new radiative transfer model for geophysical applications in the 175–2400 nm spectral region. Adv. Space Res. 36, 1015–1019, doi:10.1016/j.asr.2005.03.012, 2005.

Schanda, E. Physical Fundamentals of Remote Sensing. Springer, 1986.

Sinnhuber, B.M., Weber, M., Amankwah, A., Burrows, J.P. Total ozone during the unusual Antarctic winter of 2002. Geophys. Res. Lett. 30, 1580, doi:10.1029/2002GL016798, 2003a.

Sinnhuber, M., Burrows, J.P., Chipperfield, M.P., Jackman, C.H., Kallenrode, M., Künzi, K.F., Quack, M. A model study of the impact of magnetic field structure on atmospheric composition during solar proton events. Geophys. Res. Lett. 30, 1818, doi:10.1029/2003GL017265, 2003b.

Sitnov, S. Analysis of spatial-temporal variability of tropospheric NO_2 column over Moscow megapolis using OMI spectrometer (Aura satellite) data. Doklady Earth Sciences 429, 1511–1517, 2009.

Sudo, K., Takahashi, M., Kurokawa, J., Akimoto, H. CHASER: a global chemical model of the troposphere 1 model description. J. Geophys. Res. 107, 4339, doi:10.1029/2001JD001113, 2002.

Takigawa, M., Niwano, M., Akimoto, H., Takahashi, M. Development of a one-way nested global-regional air quality forecasting model. SOLA 3, 81–84, 2007.

van der A, R.J., Eskes, H.J., Boersma, K.F., van Noije, T.P.C., Van Roozendael, M., De Smedt, I., Peters, D.H.M.U., Meijer, E.W. Trends, seasonal variability and dominant NO_x source derived from a ten year record of NO_2 measured from space. J. Geophys. Res. 113 (D04302), doi:10.1029/2007JD009021, 2008.

Voigt, S., Orphal, J., Bogumil, K., Burrows, J.P. The temperature dependence (203–293 K) of the absorption cross sections of O_3 in the 230–850 nm region measured by Fourier-transform spectroscopy. J. Photochem. Photobiol. A: Chem. 143, 1–9, doi:10.1016/S1010-6030(01)00480-4, 2001.

Voigt, S., Orphal, J., Burrows, J.P. The temperature and pressure dependence of the absorption cross-sections of NO_2 in the 250–800 nm region measured by Fourier-transform spectroscopy. J. Photochem. Photobiol. A: Chem. 149, 1–7, doi:10.1016/S1010-6030(01)00650-5, 2002.

Volkamer, R., Spietz, P., Burrows, J.P., Platt, U. High-resolution absorption cross-section of glyoxal in the UV-vis and IR spectral ranges. J. Photochem. Photobiol. A: Chem. 172, 35–46, doi:10.1016/j.jphotochem.2004.11.011, 2005.

Wang, Y., McElroy, M.B., Boersma, K.F., Eskes, H.J., Veefkind, J.P. Traffic restrictions associated with the Sino-African summit: reductions of NO_x detected from space. Geophys. Res. Lett. 34, L08814, doi:10.1029/2007GL029326, 2007.

Witte, J.C., Schoeberl, M.R., Douglass, A.R., Gleason, J.F., Krotkov, N.A., Gille, J.C., Pickering, K.E., Livesey, N. Satellite observations of changes in air quality during the 2008 Beijing Olympics and Paralympics. Geophys. Res. Lett. 36, L17803, doi:10.1029/2009GL039236, 2009.

Zhang, Q., Streets, D.G., He, K. Satellite observations of recent power plant construction in Inner Mongolia, China. Geophys. Res. Lett. 36, L15809, doi:10.1029/2009GL038984, 2009.

Zhou, Y., Brunner, D., Spurr, R.J.D., Boersma, K.F., Sneep, M., Popp, C., Buchmann, B. Accounting for surface reflectance anisotropy in satellite retrievals of tropospheric NO_2. Atmos. Meas. Tech. 3, 1185–1203, doi:10.5194/amt-3-1185-2010, 2010.